Uniqueness of infrared asymptotics in Landau gauge Yang-Mills theory

Christian S. Fischer[1] and Jan M. Pawlowski[2]

[1]*Institut für Kernphysik, Technical University of Darmstadt, Schlossgartenstraße 9, 64289 Darmstadt, Germany*
[2]*Institut für Theoretische Physik, Universität Heidelberg, Philosophenweg 16, D-69120 Heidelberg, Germany*
(Received 7 September 2006; revised manuscript received 15 November 2006; published 12 January 2007)

We uniquely determine the infrared asymptotics of Green functions in Landau gauge Yang-Mills theory. They have to satisfy both the Dyson-Schwinger equations and functional renormalization group equations. Then, the requirement of consistency fixes the relation between the infrared power laws of these Green functions. We discuss consequences for the interpretation of recent results from lattice QCD.

DOI: 10.1103/PhysRevD.75.025012 PACS numbers: 12.38.Aw, 02.30.Rz, 05.10.Cc, 11.15.Tk

I. INTRODUCTION

In the past decade much progress has been made in the understanding of the low energy sector of QCD. This progress has been achieved both with continuum methods and lattice computations. In the continuum, nonperturbative functional methods have been used: Dyson-Schwinger equations (DSEs) and functional renormalization group equations (FRGs). Both frameworks are truly *ab initio* approaches in the sense that they can be derived rigorously from the full effective action of QCD; for reviews see [1–7]. Although both frameworks constitute an infinite hierarchy of coupled equations, they allow for the extraction of scaling laws for Green functions in the deep infrared [8–12]. These scaling laws are related to important properties of the low energy limit of QCD, such as confinement and chiral symmetry breaking.

The basic Green functions of Yang-Mills (YM) theory are the ghost and gluon propagators. In Landau gauge, these functions are connected to fundamental properties of the theory. A running coupling can be constructed from a renormalization group invariant combination of the corresponding dressing functions [8]. Furthermore, the ghost dressing function gives access to the status of global gauge symmetry: an infrared diverging ghost unambiguously signals an unbroken symmetry corresponding to a well-defined global color charge [13]. This criterion is an integral part of the Kugo-Ojima confinement scenario [14] and can be expressed as

$$p^2\langle C(p)\bar{C}(-p)\rangle \overset{p^2\to 0}{\longrightarrow} \infty, \tag{1}$$

with the ghost/antighost fields C, $\bar{C}$. It is identical to the ''horizon condition'' derived by Zwanziger [15] from considerations of the impact of the Gribov horizon on correlation functions. Within the same framework, Zwanziger also derived a remarkable condition for the gluon propagator [16],

$$\langle A(p)A(-p)\rangle \overset{p^2\to 0}{\longrightarrow} 0, \tag{2}$$

where $A(p)$ denotes the gauge field. Such an infrared vanishing gluon propagator violates the Osterwalder-Schrader axiom of reflection positivity [17] and therefore implies gluon confinement [16].

The behavior (1) and (2) has first been seen in a DSE study [8]. This result has been confirmed and extended within further DSE computations, e.g. [10,18–20], stochastic quantization, e.g. [9,21], as well as FRG computations [11,22–24]; for related work see also [25–28]. In all these studies a nonrenormalization theorem for the ghost-gluon vertex [29] is used, leading to

$$\begin{aligned} p^2\langle A(p)A(-p)\rangle &\to (p^2)^{2\kappa}, \\ p^2\langle C(p)\bar{C}(-p)\rangle &\to (p^2)^{-\kappa}, \end{aligned} \tag{3}$$

with $\kappa \in [1/2, 1[$. It has been argued in [10] that (3) is the only consistent solution. Equation (3) has been extended to a self-consistent solution of the (untruncated) tower of DSEs in continuum Yang-Mills theory [12]: for proper vertices $Z^{(2n,m)}_{0,\mathrm{as}}$ with n ghost legs, n antighost legs, and m gluon legs, the infrared asymptotics is given by

$$Z^{(2n,m)}_{0,\mathrm{as}}(p^2) \sim (p^2)^{\kappa_{(2n,m)}} \sim (p^2)^{(n-m)\kappa}, \tag{4}$$

where κ is the exponent of the ghost dressing function ($n = 1, m = 0$) as defined in (3).

It is interesting to compare the continuum result (3) with results from lattice QCD [30–37]. On the available finite volumes, most lattice results for the gluon propagator disagree with (2) in that they favor an infrared finite propagator, i.e.

$$p^2\langle A(p)A(-p)\rangle \sim (p^2)^1. \tag{5}$$

Extrapolations towards the infinite volume limit cannot yet unambiguously distinguish between an infrared finite, e.g. [38], or weakly vanishing propagator [36].

The situation is worse for the ghost dressing function. Whereas some simulations give an infrared diverging ghost [35,39], other authors interpret their results as pointing towards an infrared finite ghost dressing function [37], i.e.

$$\langle C(p)\bar{C}(-p)\rangle \sim (p^2)^0. \tag{6}$$

Clearly, (5) and (6) together do not agree with the continuum result (3). Instead, they have been proposed as a second possible solution of the continuum DSEs [37].

In this work we shall show that the infrared asymptotics of Landau gauge Yang-Mills theory is uniquely fixed by DSE and FRG. Such a combined analysis has been suggested in [7]. We first discuss the relations between these two sets of equations in the next section. Then a general infrared analysis of the DSEs for the ghost and gluon propagators as well as for the ghost-gluon vertex is performed. For illustrational purposes we rederive parts of the result (4) in a slightly different way than in the original analysis [10,12]. This allows us to also explore the consequences of the proposals (5) and (6). In the following section we perform a similar analysis within the FRG, and show that (5) and (6) cannot simultaneously solve the DSE and FRG equations. Consequently, they cannot survive the infinite volume/continuum limit of lattice gauge theory. In Sec. V we show instead that self-consistency of DSEs and FRGs enforces the unique solution (4) for the infrared asymptotics of pure Yang-Mills theory. We briefly discuss the extension of the present analysis to QCD and the electroweak sector of the standard model. In our concluding section we discuss the consequences of this result.

II. FUNCTIONAL RELATIONS

A quantum field theory or statistical theory can be defined uniquely in terms of its renormalized correlation functions. They are generated by the effective action Γ, the generating functional of 1PI Green functions. For the present work we consider pure Yang-Mills theory with the classical gauge fixed action

$$S_{\rm cl} = \frac{1}{2}\int \mathrm{tr} F^2 + \frac{1}{2\xi}\int (\partial_\mu A^\mu)^2 + \int \bar{C}\cdot\partial_\mu D_\mu \cdot C \quad (7)$$

in the presence of an additional scale k; see [7] for a detailed discussion. The propagation is modified via k-dependent terms,

$$\Delta S_k = \frac{1}{2}\int A^\mu_a R^{ab}_{\mu\nu} A^\nu_b + \int \bar{C}_a R^{ab} C_b, \quad (8)$$

where $R^{ab}_{\mu\nu}$ and R^{ab} are k-dependent regulator functions. Within the standard choice, k is an infrared cutoff scale, and the functions R cut off the propagation for momenta smaller than k. Here we also consider more general R that only have support at about the momentum scale k. Such regularizations allow for a scanning of the momentum behavior of Green functions. The regularized effective action Γ_k is expanded in gluonic and ghost vertex functions and reads schematically

$$\Gamma_k[\phi] = \sum_{m,n}\frac{1}{m!n!^2}\Gamma_k^{(2n,m)}\bar{C}^n C^n A^m, \quad (9)$$

in an expansion about vanishing fields $\phi = (A, C, \bar{C})$. In (9) an integration over momenta and a summation over indices are understood. The effective action Γ_k satisfies functional relations such as the quantum equations of motion, the DSEs; symmetry relations, the Ward or Slavnov-Taylor identities (STI); as well as functional RG or flow equations (FRGs). All these different equations relate to each other; for a detailed discussion see [7]. Indeed, the Slavnov-Taylor identities are a projection of the quantum equations of motion, whereas flow equations can be read as differential DSEs, or DSEs as integrated flows. Written as a functional relation for the effective action Γ_k, the DSE reads, e.g. [7],

$$\frac{\delta\Gamma_k}{\delta\phi}[\phi] = \frac{\delta S_{\rm cl}}{\delta\phi}[\phi_{\rm op}], \quad (10)$$

where the operators $\phi_{\rm op}$ are defined as

$$\phi_{\rm op}(x) = \int d^4y G_{\phi\phi_i}[\phi](x,y)\frac{\delta}{\delta\phi_i(y)} + \phi(x), \quad (11)$$

and

$$G_{\phi_1\phi_2}[\phi] = \left(\frac{1}{\Gamma_k^{(2)}[\phi] + R_k}\right)_{\phi_1\phi_2} \quad (12)$$

is the full field-dependent propagator for a propagation from ϕ_1 to ϕ_2. Specifying to pure YM theory, the field is given by $\phi = (A, C, \bar{C})$. The functional derivatives in (10) act on the corresponding fields and generate one-loop and two-loop diagrams in full propagators. The functional DSE (10) relates 1PI vertices, the expansion coefficients of Γ_k, to a set of one-loop and two-loop diagrams with full propagators and full vertices, but one classical vertex coming from the derivatives of $S_{\rm cl}$. We emphasize that the DSE (10) only implicitly depends on the regularization via the definition of the propagator in (12). For Yang-Mills theory a diagrammatic representation is given in Fig. 1. The rhs is given in powers of the field-dependent fully dressed propagator $G_{\phi\phi}[\phi]$, and its derivatives, as well as the field-dependent bare vertices. The momentum scaling of Green functions is directly related to the scaling of these building blocks.

The flow equation for the effective action of pure Yang-Mills theory reads [7,11]

$$\partial_t\Gamma_k[\phi] = \frac{1}{2}\int\frac{d^4p}{(2\pi)^4}G^{\mu\nu}_{ab}[\phi](p,p)\partial_t R^{ba}_{\mu\nu}(p) - \int\frac{d^4p}{(2\pi)^4}G_{ab}[\phi](p,p)\partial_t R^{ba}(p), \quad (13)$$

where $t = \ln k$. The flow (13) relates the cutoff scale derivative of the effective action to one-loop diagrams with fully dressed field-dependent propagators. We can contrast the diagrammatic representation of the DSE in Fig. 1 with that of the functional flow (13), given in Fig. 2. The rhs is given by the field-dependent fully dressed propagator $G_{\phi\phi}[\phi]$ and the regulator insertion $\partial_t R$. Here, the momentum scaling of Green functions solely depends on the scaling of G and $\partial_t R$. If we choose the regulator function R such that it has the RG and momentum scaling of the

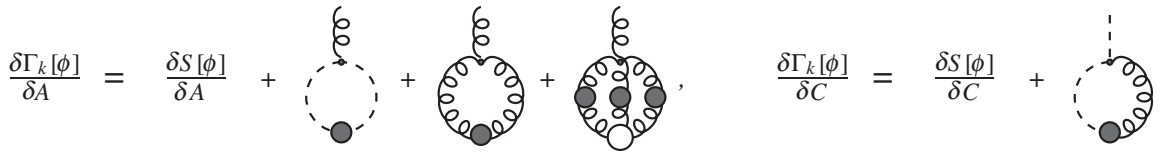

FIG. 1. Functional DSE for the effective action. Filled circles denote fully dressed field-dependent propagators (12). Empty circles denote fully dressed field-dependent vertices, and dots denote field-dependent bare vertices.

related two-point function, the flow is RG invariant [7], and only depends on full vertices and propagators, including the regulator term. The standard use of (13) is to take a regulator function $R(p^2)$ which tends towards a constant in the infrared and decays sufficiently fast in the ultraviolet, and hence implements an infrared cutoff. In the present context, there is another interesting choice for R: let R only have support at momenta p about the scale k, and $R \propto \Gamma_0^{(2)}$ at momenta $p^2 \approx k^2$. Then the regulator term does not change the theory, $\Gamma_k \simeq \Gamma_0$, and (13) only entails the (change of the) momentum dependence of Green functions of Γ_0. This provides the resolution of the momentum dependence at p^2 of the full effective action Γ_0 directly from the flow equation at $k^2 = p^2$.[1] We shall detail this choice later. It is also worth noting that the relation between DSE and FRG is natural in an NPI formulation [7], which leads to a mixture of the scaling relations derived from (10) and (13).

In the present work we investigate the leading infrared behavior of vertices and propagators constrained by the consistency of (10) and (13). Here it is important to note that the DSEs derived from (10) also depend on bare or classical vertices, whereas the flow equations derived from (13) solely depend on full vertices. In other words, both sets of equations are linked by resummations. This allows us to extract nontrivial information of the theory from a finite set of vertex DSEs and FRGs that would require a whole infinite tower of either DSEs or FRGs if restricting the analysis to either of the functional equations. We analyze the leading infrared behavior of (10) and (13) for momenta and cutoffs,

$$p^2, k^2 \ll \Lambda_{\mathrm{QCD}}^2. \tag{14}$$

To that end we introduce dressing functions $Z_k^{(2n,m)}$ for one particle irreducible Green functions with n ghost legs, n antighost legs, and m gluon legs via

$$\Gamma_k^{(2n,m)}(p_1, \ldots, p_{2n+m}) = Z_k^{(2n,m)}(p_1, \ldots, p_{2n+m}) \times \mathcal{T}^{(2n,m)}(p_1, \ldots, p_{2n+m}). \tag{15}$$

The expansion coefficients $\Gamma_k^{(2n,m)}$ of the effective action have been defined in (9). The $\mathcal{T}^{(2n,m)}$ denote the tensor structure of the respective Green functions, and carry their canonical momentum dimension. The coefficient $Z_k^{(2n,m)}$ is the dressing function of the leading infrared tensor structure. Then, following the IR analysis in [11,24], the asymptotic vertex functions can be expanded about the leading asymptotics at a vanishing cutoff $k = 0$:

$$Z_k^{(2n,m)}(p_1, \ldots, p_{2n+m}) = Z_{0,\mathrm{as}}^{(2n,m)}(p_1, \ldots, p_{2n+m}) \times (1 + \delta Z^{(2n,m)}(\hat{p}_1, \ldots, \hat{p}_{2n+m})), \tag{16}$$

where $\hat{p}_i = p_i/k$, and the asymptotic infrared part $Z_{0,\mathrm{as}}^{(2n,m)}$ only depends on ratios of monomials and possible logarithmic dependencies. Inserting the parametrization (16) into the flow (13) and solving for $\delta Z^{(2n,m)}$, one can prove that $\delta Z^{(2n,m)}$ solely depends on $\hat{p}_i$. This suffices to fix the relations between the anomalous scalings of the vertex functions $Z_{0,\mathrm{as}}^{(2n,m)}$ independent of the $\delta Z^{(2n,m)}$.

In our analysis we are only interested in the global scaling behavior for the dressing functions $Z_0^{(2n,m)}$, that is, modulo logarithmic scaling,

$$Z_{0,\mathrm{as}}^{(2n,m)}(\lambda p_1, \ldots, \lambda p_{2n+m}) = \lambda^{\kappa_{2n,m}} Z_{0,\mathrm{as}}^{(2n,m)}(p_1, \ldots, p_{2n+m}). \tag{17}$$

We emphasize that, in principle, additional logarithmic scalings should be included in (17). However, even if present, additional logarithmic scalings do not change the relations between the $\kappa_{n,m}$ and are therefore irrelevant for the purpose of the present investigation. We also add that, in practice, self-consistent logarithmic scaling laws are hardly possible and have not been found yet.

Specifically interesting for the Kugo-Ojima/Gribov-Zwanziger confinement scenario are the exponents $\kappa_{0,2}$ and $\kappa_{2,0}$ of the inverse gluon dressing function $Z^{(0,2)}$ and inverse ghost dressing function $Z^{(2,0)}$. The conditions (1) and (2) read

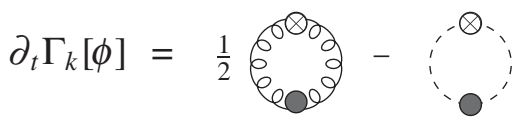

FIG. 2. Functional flow for the effective action. Filled circles denote fully dressed field-dependent propagators (12). Crosses denote the regulator insertion $\partial_t R$.

[1]Such a single mode regulator cannot be used to solve the theory by successively integrating out degrees of freedom. However, it proves useful for studying fixed point solutions [40].

$$\kappa_{2,0} > 0, \qquad \kappa_{0,2} < -1. \tag{18}$$

We close this section with a remark on the interpretation of the scaling analysis derived from the combined functional relations (10) and (13). In principle, such an analysis produces the most singular scaling of all diagrams involved and is not sensitive to either the cancellations between different diagrams or to cancellations within a given diagram. However, to affect the infrared behavior of the Green functions in a consistent way, such cancellations have to work in the whole tower of DSEs and FRGs and therefore can only be driven by symmetries. In the present case we consider such a possibility as highly unlikely. We will come back to these points at the end of Sec. V.

III. INFRARED ANALYSIS OF THE GHOST AND GLUON DSES

The Dyson-Schwinger equations for the ghost and gluon propagators are given diagrammatically in Fig. 3. The infrared behavior of these propagators can be analyzed as follows [9,10,12,41]: We choose the external momentum scale p^2, according to (14), to be much smaller than any other scale, i.e. $p^2 \ll \Lambda_{\rm QCD}$, where $\Lambda_{\rm QCD} \sim \mathcal{O}(200\ {\rm MeV})$ is the nonperturbative scale of Yang-Mills theory generated via dimensional transmutation. The loop integrals on the right-hand side of the DSEs are dominated by momentum configurations, where the internal loop momentum q is of the same order as the external momentum, i.e. $p^2 \sim q^2$. The reason for this well-known behavior is the appearance of at least one propagator in each loop with a denominator proportional to $(p-q)^2$. Thus a self-consistent solution of the equations with a small external momentum can be obtained by replacing all dressing functions inside the loops with their infrared asymptotic behavior.

We exemplify this analysis with the ghost DSE. For the sake of comparison with the literature, we switch to the standard DSE notation, where the nonperturbative dressing

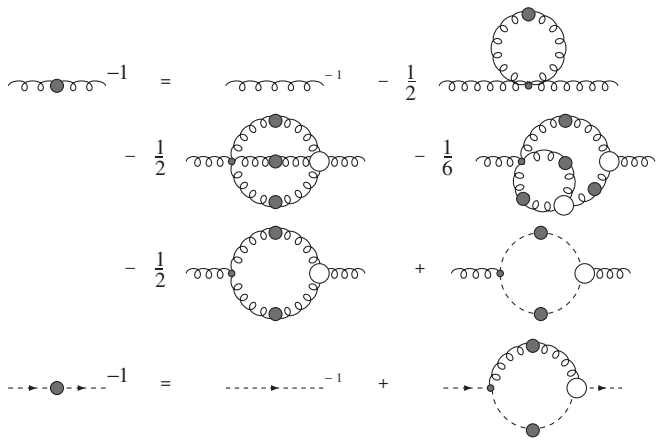

FIG. 3. Dyson-Schwinger equations for the gluon and ghost propagator. Filled circles denote dressed propagators, and empty circles denote dressed vertex functions.

of the propagators is denoted by propagator dressing functions $G(p^2)$ and $Z(p^2)$:

$$\frac{1}{Z_0^{(2,0)}(p^2)} = G(p^2), \qquad \frac{1}{Z_0^{(0,2)}(p^2)} = Z(p^2), \tag{19}$$

and Zwanziger's conditions (18) read

$$\lim_{p^2\to 0} G(p^2) = \infty, \qquad \lim_{p^2\to 0} \frac{Z(p^2)}{p^2} = 0. \tag{20}$$

The DSE for the ghost propagator is given by

$$\frac{1}{G(p^2)} = \tilde{Z}_3 - g^2 N_c \int \frac{d^4q}{(2\pi)^4} \times \frac{G(q^2)Z(l^2)}{p^2 q^2 l^2}\, p\mathcal{P}(l)q Z_0^{(2,1)}(p,q), \tag{21}$$

with the momentum routing $l = (q-p)$. The abbreviation $p\mathcal{P}(l)q$ denotes a contraction with the transverse momentum tensor $p\mathcal{P}(l)q = p_\mu P_{\mu\nu}(l) q_\nu$, and $Z_0^{(2,1)}(p,q)$ denotes the dressing of the ghost-gluon vertex. The ghost renormalization constant $\tilde{Z}_3$ absorbs all ultraviolet divergencies from the loop integral, thus rendering the right-hand side of the equation UV finite. This can be made explicit within a momentum subtraction scheme. Here $\tilde{Z}_3$ is evaluated at a subtraction point $p^2 = \mu^2$, which we choose to be $\mu^2 = 0$. One obtains

$$\tilde{Z}_3 = \frac{1}{G(0)} + g^2 N_c \int \frac{d^4q}{(2\pi)^4} \frac{3}{4} \frac{G(q^2)Z(q^2)}{q^4} Z_0^{(2,1)}(0,q), \tag{22}$$

and subsequently

$$\frac{1}{G(p^2)} = \frac{1}{G(0)} - g^2 N_c \int \frac{d^4q}{(2\pi)^4} \times \left\{ \frac{G(q^2)Z(l^2)}{p^2 q^2 l^2}\, p\mathcal{P}(l)q Z_0^{(2,1)}(p,q) + \frac{3}{4} \frac{G(q^2)Z(q^2)}{q^4} Z_0^{(2,1)}(0,q) \right\}. \tag{23}$$

Now the integral is UV finite and we replace the dressing functions in the loop by their infrared expansion in terms of the power laws

$$Z(p^2) \sim (p^2)^{-\kappa_{0,2}}, \qquad G(p^2) \sim (p^2)^{-\kappa_{2,0}}, \qquad Z_0^{(2,1)}(p,q) \sim (q^2)^{\kappa_{2,1}}. \tag{24}$$

Here it does not matter whether the vertex function $Z_0^{(2,1)}$ is represented by powers of (q^2), (l^2) or, more realistically, by powers of $(p^2+q^2+l^2)$. The crucial point is that after integration all powers of internal loop momenta will be transformed into powers of the only external scale p^2 for dimensional reasons. This can be seen easily for the expansion (24), which leads to integrals that can be performed employing

$$\int d^4q \frac{(q^2)^a (l^2)^b}{q^2 l^2} = \pi^2 \frac{\Gamma(1+a)\Gamma(1+b)\Gamma(-a-b)}{\Gamma(1-a)\Gamma(1-b)\Gamma(2+a+b)} \times (p^2)^{a+b}. \quad (25)$$

Plugging (24) into (23), performing the integration and matching with the left-hand side, $1/G(p^2) \sim (p^2)^{\kappa_{2,0}}$, we obtain two self-consistent solutions:

$$(p^2)^{\kappa_{2,0}} \sim \begin{cases} (p^2)^{-\kappa_{0,2}-\kappa_{2,0}+\kappa_{2,1}}, \\ (p^2)^0. \end{cases} \quad (26)$$

In the first case, the loop integral dominates the right-hand side, and the constant $1/G(0)$ is canceled by other terms (see [10] for a detailed discussion). In the second case, this constant does not vanish and dominates the right-hand side of the equation in the infrared. We thus end up with two possible conditions:

$$\kappa_{2,0} \sim \begin{cases} -\frac{1}{2}\kappa_{0,2} + \frac{1}{2}\kappa_{2,1}, \\ 0, \end{cases} \quad (27)$$

from the ghost DSE. Either $G(0)$ is divergent, in accordance with the horizon condition (20), or it is finite as proposed in [37] and violates (20). Strong arguments against the latter possibility have been discussed in [10,42], where it has been concluded that $\kappa_{2,0} > 0$. For the sake of argument, however, we will not use this result here but proceed by exploring the consequences of both options.

We would like to stress again that we could have obtained the solutions (27) without explicitly solving the loop integral: since the external momentum (p^2) is the only scale in our problem, all powers of internal momenta in the loop have to translate into powers of external momenta after integration for dimensional reasons. Thus, by simply counting the infrared exponents of all loop propagators and vertices, we also arrive at (27).

We proceed by analyzing the DSE for the gluon propagator. Schematically we can write this equation as

$$\frac{1}{Z(p^2)} = Z_3 + \Pi_{\text{tadpole}}(p^2) + \Pi_{\text{sunset}}(p^2) + \Pi_{\text{squint}}(p^2) + \Pi_{\text{gluon loop}}(p^2) + \Pi_{\text{ghost loop}}(p^2), \quad (28)$$

where the dressing loops appear in the same order as in Fig. 3. The static tadpole term is absorbed in the process of renormalization. We therefore have to analyze the infrared behavior of the four remaining dressing loops. Counting IR exponents in the loops, we arrive at

$$\begin{aligned} \Pi_{\text{sunset}}(p^2) &\sim (p^2)^{-3\kappa_{0,2}+\kappa_{0,4}}, \\ \Pi_{\text{squint}}(p^2) &\sim (p^2)^{-4\kappa_{0,2}+2\kappa_{0,3}}, \\ \Pi_{\text{gluon loop}}(p^2) &\sim (p^2)^{-2\kappa_{0,2}+\kappa_{0,3}}, \\ \Pi_{\text{ghost loop}}(p^2) &\sim (p^2)^{-2\kappa_{2,0}+\kappa_{2,1}}. \end{aligned} \quad (29)$$

The infrared leading term from the right-hand side has to match the left-hand side $1/Z(p^2) \sim (p^2)^{\kappa_{0,2}}$ of the DSE. We thus obtain the expression

$$\kappa_{0,2} = \min(0, -3\kappa_{0,2} + \kappa_{0,4}, -4\kappa_{0,2} + 2\kappa_{0,3}, -2\kappa_{0,2} + \kappa_{0,3}, -2\kappa_{2,0} + \kappa_{2,1}), \quad (30)$$

and subsequently

$$\kappa_{0,2} = \min\left(0, \tfrac{1}{4}\kappa_{0,4}, \tfrac{2}{5}\kappa_{0,3}, \tfrac{1}{3}\kappa_{0,3}, -2\kappa_{2,0} + \kappa_{2,1}\right), \quad (31)$$

as our final condition for the gluon exponent $\kappa_{0,2}$ from the gluon DSE. In general, we expect $\kappa_{0,2} < 0$ according to the Kugo-Ojima and horizon conditions (1) and (20) and lattice QCD (see e.g. [38]). It is interesting to note that for negative $\kappa_{0,2}$ the contribution from the gluon loop, $1/3\kappa_{0,3}$, is never the leading one on the right-hand side of (30), since it is always dominated by the contribution from the squint diagram, $2/5\kappa_{0,3}$. Thus any truncation of the gluon DSE that assumes a leading gluon loop (see e.g. [43–45]) is in fact missing the dominant contribution in the infrared.

A further crucial ingredient is the DSE for the ghost-gluon vertex. One version is derived from the DSE for $\delta\Gamma/\delta A$, and is given diagrammatically in Fig. 4. Similarly to the ghost and gluon propagator DSE, we arrive at

$$\kappa_{2,1} \leq \min(2\kappa_{2,0} + \kappa_{0,2}, 2\kappa_{0,2} + \kappa_{2,0}, \kappa_{2,2} - 2\kappa_{0,2}, \kappa_{4,0} - 2\kappa_{2,0}). \quad (32)$$

The inequality takes into account that the exponents of the two-loop diagrams in the vertex DSE may even be smaller than those of the one-loop diagrams considered in (32).[2] From (32) we conclude that

$$\kappa_{2,1} \leq 2\kappa_{2,0} + \kappa_{0,2}. \quad (33)$$

Equation (33) together with the FRG relation derived in the next section suffices to uniquely fix the relations between all $\kappa_{2n,m}$ in a closed form.

Based on the conditions (27) and (31) and the exact equality in (33), an infrared analysis of the DSEs for the three-gluon vertex and the four-gluon vertex has been performed in [12]. These results have been generalized to any Green function with n external ghost legs, n antighost legs, and m gluon legs:

$$Z^{(2n,m)}_{0,\text{as}}(p^2) \sim (p^2)^{(n-m)\kappa}, \quad (34)$$

with $\kappa = \kappa_{2,0} > 0$. This expression solves (27) and (31) and any other condition from the higher DSEs. In addition, it solves the Slavnov-Taylor identities. Important aspects of this solution are discussed in detail in [3]. Two of the characteristic properties of (34) are that (i) contributions

[2] $\kappa_{2,1}$ can also be determined from the DSE for $\delta\Gamma/\delta C$ or $\delta\Gamma/\delta\bar{C}$; see Fig. 1. However, the present analysis then turns out to be more complicated even though two-loop terms are absent.

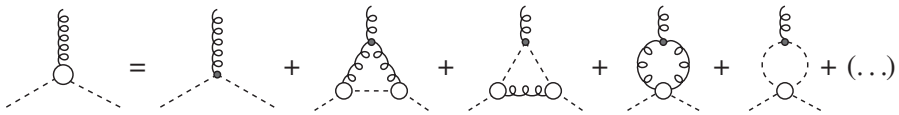

FIG. 4. Dyson-Schwinger equation for the ghost-gluon vertex, derived via Eq. (10). All internal propagators are taken to be fully dressed. The ellipsis denotes two-loop diagrams, which are not needed for our analysis.

from ghost loops always dominate the DSEs and (ii) it leads to IR-fixed points in the running couplings from the ghost-gluon (gh), three-gluon ($3g$), and four-gluon vertices ($4g$). These couplings are defined via

$$\alpha^{gh}(p^2) = \frac{g^2}{4\pi}[Z_0^{(2,1)}(p^2)]^2 G^2(p^2) Z(p^2), \tag{35a}$$

$$\alpha^{3g}(p^2) = \frac{g^2}{4\pi}[Z_0^{(0,3)}(p^2)]^2 Z^3(p^2), \tag{35b}$$

$$\alpha^{4g}(p^2) = \frac{g^2}{4\pi}[Z_0^{(0,4)}(p^2)] Z^2(p^2), \tag{35c}$$

where $Z_0^{-1} = Z_0^{(0,2)}$ and $G^{-1} = Z_0^{(2,0)}$. The vertex dressing functions $Z_0^{(2,1)}(p_1, p_2, p_3)$, $Z_0^{(0,3)}(p_1, p_2, p_3)$, and $Z_0^{(0,4)}(p_1, p_2, p_3)$ are evaluated at the symmetric momentum point $p_1^2 = p_2^2 = p_3^2 = p^2$, which makes them functions of p^2 only.

From the tower of DSEs alone, it is difficult to prove that (34) is unique. One way to search for a second possible solution would be to assume $\kappa_{2,0} = 0$ and $\kappa_{0,2} = -1$ from the start, corresponding to the behavior (5) and (6), as proposed in [37]. From Eqs. (27) and (31) one obtains consistency provided that one of the three vertices is strongly divergent:

$$\kappa_{2,1} = -1 \quad \text{or} \quad \kappa_{0,3} = -5/2 \quad \text{or} \quad \kappa_{0,4} = -4. \tag{36}$$

In the next section we will show that all options (36) lead to inconsistencies in the functional renormalization group equations.[3] As discussed in Sec. II, any solution of the tower of DSEs necessarily has to solve the tower of FRGs as well. This provides tight constraints on possible solutions, which are in fact sufficient to prove the uniqueness of (34), as we shall see.

IV. INFRARED ANALYSIS OF GHOST AND GLUON FLOWS

Now we repeat the infrared analysis within the FRG framework; see [11,23,24]. We restrict ourselves to regulator functions of the form

$$R_k(p^2) = \Gamma_k^{(2)}(p^2) r(p^2/k^2), \tag{37}$$

where $\Gamma_k^{(2)}$ is the corresponding two-point function $\Gamma_k^{(2,0)}$ for the ghost, and $\Gamma_k^{(0,2)}$ for the gluon. Regulator functions (37) guarantee the persistence of the standard RG scalings in the presence of an IR cutoff, and are therefore best-suited for the present studies. Within the parametrization (16) and as a consequence of (37), propagators $G_{\phi_1\phi_2}(p^2)$ take the asymptotic form

$$G_{\phi_1\phi_2}(p^2) = \frac{1}{\Gamma_k^{(2)}(p^2)} \frac{1}{1 + r(\hat{p}^2)} \simeq \frac{1}{\Gamma_{0,\mathrm{as}}^{(2)}(p^2)} \frac{1}{1 + \delta Z^{(2)}(\hat{p})} \frac{1}{1 + r(\hat{p}^2)}, \tag{38}$$

where $\Gamma_{0,\mathrm{as}}^{(2)}$ is the leading infrared asymptotics of the two-point function at a vanishing cutoff $k = 0$. Equation (38) can be solely written in terms of $\hat{p}$ and k dependences. Then it reads

$$G_{\phi_1\phi_2}(p^2) = \frac{1}{k^{2(1+\kappa)}} \frac{1}{\Gamma_{0,\mathrm{as}}^{(2)}(\hat{p}^2)} \frac{1}{1 + \delta Z^{(2)}(\hat{p})} \frac{1}{1 + r(\hat{p}^2)}, \tag{39}$$

where κ is either $\kappa_{0,2}$ (gluon) or $\kappa_{2,0}$ (ghost). The same rescaling can be done with all vertex functions:

$$\Gamma_k^{(2n,m)}(p_1, \ldots, p_{2n+m}) \simeq k^{2(d_{n,m}+\kappa_{2n,m})} \Gamma_{0,\mathrm{as}}^{(2n,m)}(\hat{p}_1, \ldots, \hat{p}_{2n+m}) \times (1 + \delta Z^{(2n,m)}(\hat{p}_1, \ldots, \hat{p}_{2n+m})), \tag{40}$$

where $d_{n,m}$ carries the canonical momentum dimension, e.g. $d_{2,0} = d_{0,2} = 1$, and $\Gamma_{0,\mathrm{as}}^{(2n,m)}$ is the leading infrared asymptotics of the $(2n, m)$-point function at a vanishing cutoff $k = 0$. One can already read off crucial information from (40): the leading momentum scaling of the dressing function is identical to its leading k scaling.

An interesting specific choice for (37) is a regulator function R_k that only has support for momenta at about k^2:

$$R_k(p^2) = \Gamma_0^{(2)}(p^2) \delta_\epsilon(p^2 - k^2), \tag{41}$$

where $\delta_\epsilon(x)$ is proportional to a smeared-out δ function at $x = 0$, and the $\delta Z^{(2n,m)}$ only have support at momenta $p_i^2 \approx k^2$. With regulators (41), the momentum dependence of $\Gamma_k^{(2n,m)}$ agrees with that of $\Gamma_0^{(2n,m)}$, and hence (41) falls into the class (37). For regulators (41) only the *strength* of the two-point function $\Gamma_k^{(2)} \simeq \Gamma_0^{(2)}$ in the momentum window $p^2 \approx k^2$ is changed. In particular, the infrared power laws at $k \neq 0$ agree with those at $k = 0$. Therefore we can directly read off the momentum dependence at the momentum scale $p^2 = k^2$.

[3]Note that the second option together with (35b) leads to a strongly divergent running coupling, $\alpha^{3g} \sim 1/p^2$, which appears to disagree with the lattice results of [46].

However, for a quantitative comparison of FRG with DSE beyond the infrared power laws, the theory has to be solved explicitly in both approaches. For the FRG this is only possible with regulators (37) that provide a momentum cutoff, in contrast to (41). Hence we proceed with a true momentum regulator with (37). Within the parametrization (40), integrated asymptotic flows for general vertices read

$$\Gamma^{(2n,m)}_{0,\mathrm{as}}(p_1,\ldots,p_{2n+m})\delta Z^{(2n,m)}(\hat{p}_1,\ldots,\hat{p}_{2n+m}) \simeq \int_0^k \frac{dk'}{k'}\,\partial_t\Gamma^{(2n,m)}_k(p_1,\ldots,p_{2n+m}), \tag{42}$$

where the left-hand side follows from the representation (16) as the difference $\Gamma^{(2n,m)}_k - \Gamma^{(2n,m)}_0$. The leading momentum dependence on both sides has to agree. Within an iteration about $\delta Z^{(n,m)} = 0$ on the right-hand side (rhs) of (42), one can indeed prove that $\delta Z^{(n,m)}$ is a function of $\hat{p}_i = p_i/k$ [11]. Consequently, dividing the equation by $\Gamma^{(2n,m)}_{0,\mathrm{as}}$ leads to an equation only depending on ratios $\hat{p}_i = p_i/k$. Hence we arrive at

$$\delta Z^{(2n,m)}(\hat{p}_1,\ldots,\hat{p}_{2n+m}) \simeq \int_0^k \frac{dk'}{k'}\left(\frac{1}{\Gamma^{(2n,m)}_{0,\mathrm{as}}}\,\partial_t\Gamma^{(2n,m)}_k\right) \times(\hat{p}'_1,\ldots,\hat{p}'_{2n+m}), \tag{43}$$

where we have dropped the subleading terms. Equation (43) defines consistently renormalized finite DSEs [7]. In contrast to the DSEs (10), it solely depends on full vertices but also involves an integration over the cutoff scale k. The term $\partial_t\Gamma^{(2n,m)}$ on the rhs of (43) is derived by taking $(2n, m)$ derivatives of the rhs of the flow (13), leading to a sum of one-loop diagrams with dressed vertices and dressed propagators. For vertices with $\kappa_{2n,m} < 0$, we have

$$\delta Z^{(2n,m)}(0,\ldots,0) = -1. \tag{44}$$

Equation (44) simply entails that an infrared cutoff is present and the divergent infrared behavior for $k = 0$ is suppressed. From (44) we derive a relation between the involved $\kappa_{i,j}$ with $i,\ j \leq n+1,\ m+2$ in the flow of $\Gamma^{(2n,m)}_k$. The analysis for $\kappa_{2n,m} \geq 0$ within the integrated flow (43) is slightly more involved. This is in one-to-one correspondence to possible difficulties with bare terms in the DSEs. However, as outlined above we can also directly resolve the momentum behavior from (13) with regulators (41), where these problems are absent. In fact, this procedure already eliminates the possibility of solely dominating bare terms in the DSEs.

We proceed with the analysis of the propagator FRGs. For a classical vertex structure this analysis has been put forward in [11]. The results for the propagator κ's and α_s are identical to the analytical results from DSE and stochastic quantization [9,10]. Moreover, it has been proven in [11] that the integrated FRGs in this truncation result in a consistent Bogoliubov-Parasuik-Hepp-Zimmerman (BPHZ)-type renormalization procedure for the related DSE equations. Such a procedure eliminates any ambiguity due to the appearance of bare and dressed vertices in the DSEs. It has been extended to general truncation schemes in [7], and sustains general truncated DSEs with a fully consistent UV renormalization. In combination, the DSE and FRG results show that the classical vertex truncation is self-consistent, and also quantitatively reliable.

Now we perform the consistency analysis of the full theory. The propagator FRGs can be derived from Fig. 2 and are shown diagrammatically in Fig. 5.

We exemplify the analysis at the gluon propagator with $\kappa_{0,2} < 0$. As $\delta Z^{(0,2)}$ has to approach -1, the momentum scaling of the k integral in (43) has to precisely cancel that of $1/\Gamma^{(0,2)}_{0,\mathrm{as}}$. On the rhs of (43) we can iterate the full $\Gamma^{(2n,m)}_k$ about those at $k = 0$, $\Gamma^{(2n,m)}_{0,\mathrm{as}}$. Consequently, we can sum over the $\kappa_{2n,m}$ to identify the leading $\hat{p}$ behavior. With the regulator (41), this follows directly. Within this choice we have $\Gamma^{(2n,m)}_k \propto \Gamma^{(2n,m)}_{0,\mathrm{as}}$ in the flow, and the relations between the $\kappa_{2n,m}$ are derived from simply counting powers of momenta. Schematically, in Fig. 5 the first two ghost terms for the integrated flow (42) of the gluon propagator read

$$\delta Z^{(0,2)}(\hat{p}) \simeq -\frac{1}{Z^{(0,2)}_{0,\mathrm{as}}(p^2)}\,\frac{g^2N_c}{3}\int_0^k\frac{dk'}{k'}\int\frac{d^4q}{(2\pi)^4}\,\frac{q\mathcal{P}(p)q}{p^2q^2l^2} \times\frac{Z^{(2,1)}_{0,\mathrm{as}}(p,q,l)}{Z^{(2,0)}_{0,\mathrm{as}}(q^2)}\,\frac{Z^{(2,1)}_{0,\mathrm{as}}(p,l,q)}{Z^{(2,0)}_{0,\mathrm{as}}(l^2)} \times\partial_t\left(\frac{1}{1+r(\hat{q}'^2)}\,\frac{1}{1+r(\hat{l}'^2)}\right)+\cdots, \tag{45}$$

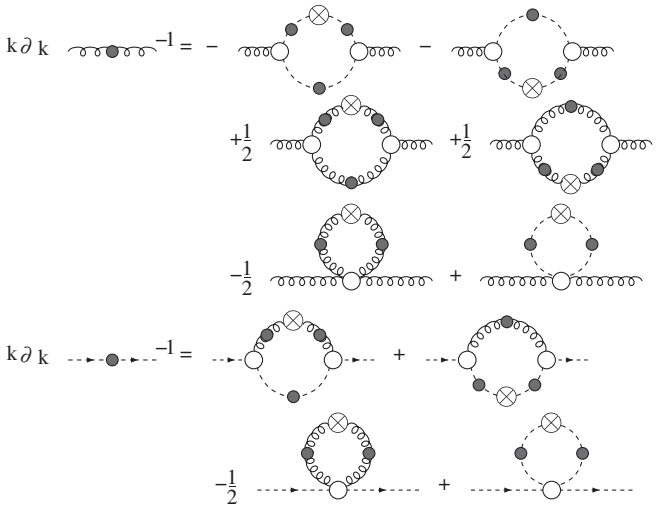

FIG. 5. Functional renormalization group equations for the gluon and ghost propagator. Filled circles denote dressed propagators, and empty circles denote dressed vertex functions. Crosses indicate insertions of the infrared cutoff function.

where we have dropped the δZ-terms on the rhs, $l = (q - p)$, $\hat{q}' = q/k'$, and the dots stand for the remaining diagrams in Fig. 5 and subleading terms. The full result can be reinstated within an iteration about $\delta Z = 0$. Note also that $\delta Z \neq 0$ for momenta which are suppressed by the regulator on the rhs. The k' integration is easily performed and leaves us with

$$\delta Z^{(0,2)}(\hat{p}) \sim \frac{1}{Z^{(0,2)}_{0,\mathrm{as}}(p^2)} \frac{g^2 N_c}{3} \int \frac{d^4q}{(2\pi)^4} \frac{q\mathcal{P}(p)q}{p^2 q^2 l^2} \times \frac{Z^{(2,1)}_{0,\mathrm{as}}(p,q,l)}{Z^{(2,0)}_{0,\mathrm{as}}(q^2)} \frac{Z^{(2,1)}_{0,\mathrm{as}}(p,l,q)}{Z^{(2,0)}_{0,\mathrm{as}}(l^2)} \times \left(1 - \frac{1}{1 + r(\hat{q}^2)} \frac{1}{1 + r(\hat{l}^2)}\right) + \cdots. \quad (46)$$

The first and second lines in (46) equals the DSE contribution if one of the vertex dressings is put to 1:

$$(Z^{(2,1)}_{0,\mathrm{as}})^2 \to Z^{(2,1)}_{0,\mathrm{as}}. \quad (47)$$

The third line produces a BPHZ-type UV renormalization, and thus furnishes a consistent RG scheme for truncated DSEs. It does not interfere with the infrared asymptotics. Hence the leading infrared behavior can be extracted from the first line in (46). Using the infrared power laws (24), we conclude that

$$\kappa_{0,2} \leq 2\kappa_{2,1} - 2\kappa_{2,0}. \quad (48)$$

The inequality originates in the left-out diagrams that could lead to a more divergent infrared asymptotics. The inclusion of δZ contributions does not change the relation (48), but changes the numerical value of the κ's. For a given truncation to the full FRGs, this leads to a regulator dependence of the results which can be used to estimate the reliability of the truncation invoked. However, it can be shown that within a given truncation scheme a functional optimization [7] implies that δZ does not contribute to the momentum integrals for optimal regulators [7]. It is precisely this optimization which led to results identical to the DSE results in the same truncation [11].

Repeating the above analysis for the remaining diagrams of the gluon FRG in Fig. 5, we are led to the relation

$$\kappa_{0,2} = \min(2\kappa_{2,1} - 2\kappa_{2,0}, 2\kappa_{0,3} - 2\kappa_{0,2}, \kappa_{0,4} - \kappa_{0,2}, \kappa_{2,2} - \kappa_{2,0}), \quad (49)$$

which can be solved for $\kappa_{0,2}$,

$$\kappa_{0,2} = \min\left(2\kappa_{2,1} - 2\kappa_{2,0}, \tfrac{2}{3}\kappa_{0,3}, \tfrac{1}{2}\kappa_{0,4}, \kappa_{2,2} - \kappa_{2,0}\right). \quad (50)$$

Equation (50) is already sufficient to rule out all three options in (36). Indeed, if we insert (36) into (50) we arrive at

$$\kappa_{0,2} \leq \begin{cases} -2, \\ -\frac{5}{3}, \\ -2, \end{cases} \quad (51)$$

for the three options. However, (36) goes with $\kappa_{0,2} = -1$. The behavior (5) and (6), proposed in [37], is therefore ruled out.

Now we use the combined DSE-FRG analysis to uniquely determine the κ's without any further input. We shall see that a self-consistent solution leads to $\kappa_{2,1} = 0$. To that end we also discuss the derivation of the κ's for the ghost propagator and the ghost-gluon vertex. For general regulators the infrared analysis for the ghost propagator is intricate and we defer the reader to [11,24]. With the choice (41) the result follows directly from the flow of the ghost propagator. Analogously to (50) we get from Fig. 5

$$\kappa_{2,0} = \min(\kappa_{2,1} - \tfrac{1}{2}\kappa_{0,2}, \kappa_{2,2} - \kappa_{0,2}, \tfrac{1}{2}\kappa_{4,0}). \quad (52)$$

The FRG relations (50) and (52) as well as the DSE relations (27) and (31) for $\kappa_{2,0}$ and $\kappa_{0,2}$ are not closed, as they also depend on vertex kappa's. The ghost-gluon vertex comprises the crucial information. It is protected by non-renormalization which turns out to be powerful enough to fix the whole system completely. Its flow is given by all one-loop diagrams with regulator insertions and full vertices (up to five-point vertices) with one external gluon line, one ghost line, and one antighost line. Its flow is given schematically in Fig. 6.

The infrared analysis of Fig. 6 with (43), or alternatively employing (41), leads to

$$\kappa_{2,1} = \min(2\kappa_{0,2} + \kappa_{2,0} - \kappa_{0,3}, \tfrac{1}{2}\kappa_{0,2} + \kappa_{2,0}, \kappa_{0,3} + \kappa_{2,2} - 2\kappa_{0,2}, \kappa_{4,1} - \kappa_{2,0}, \kappa_{2,3} - \kappa_{0,2}), \quad (53)$$

from Figs. 6(a)–6(c), 6(f), and 6(g), respectively. Figures 6(d) and 6(e) involve exactly one ghost-gluon vertex, and the related anomalous scaling cancels on both sides of Fig. 6. The surviving κ's cannot be negative, as this

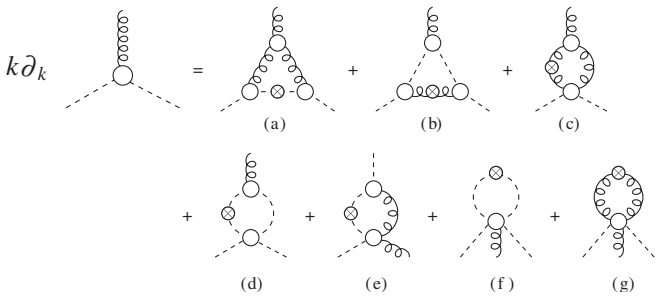

FIG. 6. Functional renormalization group equations for the ghost-gluon vertex. All propagators and vertices are fully dressed. Only one possible insertion of the infrared cutoff function per diagram is shown.

spoils the self-consistency of the integrated flow. Hence Figs. 6(d) and 6(e) lead to the constraints

$$\kappa_{4,0} - 2\kappa_{2,0} \geq 0, \tag{54a}$$

$$\kappa_{2,2} - \kappa_{0,2} - \kappa_{2,0} \geq 0. \tag{54b}$$

Additionally, the nonrenormalization of the ghost-gluon vertex [29] constrains

$$\kappa_{2,1} \leq 0, \tag{55}$$

as at least one tensor structure of the ghost-gluon vertex has a finite dressing. From the second term on the rhs of (53), we extract

$$\kappa_{2,1} \leq \tfrac{1}{2}\kappa_{0,2} + \kappa_{2,0}. \tag{56}$$

We insert (56) in the first term of (49) and arrive at $\kappa_{0,2} \leq \kappa_{0,2}$. Consequently, the bound in (56) has to be saturated and

$$\kappa_{2,1} = \tfrac{1}{2}\kappa_{0,2} + \kappa_{2,0}. \tag{57}$$

The DSE analysis leads to the constraint $\kappa_{2,1} \leq \kappa_{0,2} + 2\kappa_{2,0}$, (33). With (57) this turns into $\kappa_{2,1} \leq 2\kappa_{2,1}$. As $\kappa_{2,1} \leq 0$, (55), we arrive at the unique solution

$$\kappa_{2,1} = 0, \tag{58}$$

accompanied by the relation

$$\kappa_{0,2} = -2\kappa_{2,0}, \tag{59}$$

for the dressing of ghost and gluon propagators in agreement with [8].

V. UNIQUENESS OF INFRARED ASYMPTOTICS

The analysis of the last two sections for the propagators and the ghost-gluon vertex can be extended to all $\kappa_{n,m}$. We first derive the relations for the purely gluonic three- and four-point functions. The flow of three- and four-gluon vertices is given by all one-loop diagrams with regulator insertions and full vertices (up to five- and six-point vertices, respectively). For the three-gluon vertex the flow is given schematically in Fig. 7.

Using Fig. 7 we arrive at

$$\kappa_{0,3} = \min(\tfrac{3}{2}\kappa_{0,2}, 3\kappa_{2,1} - 3\kappa_{2,0}, \kappa_{2,2} + \kappa_{2,1} - 2\kappa_{2,0}, \kappa_{2,3} - \kappa_{2,0}, \kappa_{0,5} - \kappa_{0,2}), \tag{60}$$

from Figs. 7(a), 7(b), and 7(d)–7(f). Figure 7(c) leads to the constraint

$$\kappa_{0,4} - 2\kappa_{0,2} \geq 0, \tag{61}$$

which already restricts the singular behavior of the four-gluon vertex. We also remark that (60) puts a simple upper bound on $\kappa_{0,3}$, namely

$$\kappa_{0,3} \leq \tfrac{3}{2}\kappa_{0,2}. \tag{62}$$

This bound is the natural scaling of the vertex in the presence of a fixed point for the coupling constant α_s. Note, however, that *a priori* not all couplings as defined in (35) run to a fixed point.

The same analysis can be done for the four-gluon vertex. Its flow is given schematically in Fig. 8.

Similarly as for the three-gluon vertex, we derive from Fig. 8 the anomalous scaling of the four-gluon vertex,

$$\begin{aligned}\kappa_{0,4} = \min(&4\kappa_{0,3} - 4\kappa_{0,2}, 4\kappa_{2,1} - 4\kappa_{2,0}, \kappa_{0,5} + \kappa_{0,3} - 2\kappa_{0,2}, \kappa_{2,3} + \kappa_{2,1} - 2\kappa_{2,0}, 2\kappa_{0,2}, 2\kappa_{2,2} \\ &- 2\kappa_{2,0}, \kappa_{0,6} - \kappa_{0,2}, \kappa_{2,4} - \kappa_{2,0}, \kappa_{2,2} + 2\kappa_{2,1} - 3\kappa_{2,0}),\end{aligned} \tag{63}$$

from Figs. 8(a)–8(h) and 8(j), respectively. Figure 8(i) leads to the constraint

$$2\kappa_{0,3} - 3\kappa_{0,2} \geq 0. \tag{64}$$

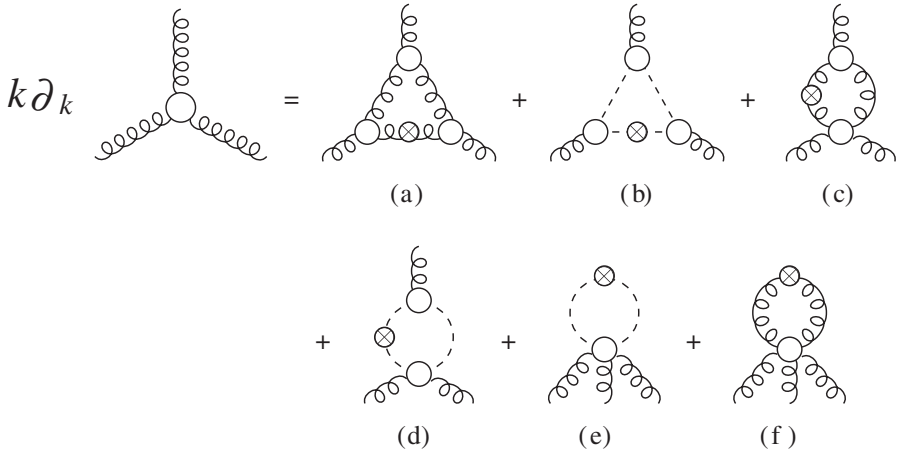

FIG. 7. Functional renormalization group equations for the three-gluon vertex. All internal propagators are taken to be fully dressed. Only one possible insertion of the infrared cutoff function per diagram is shown.

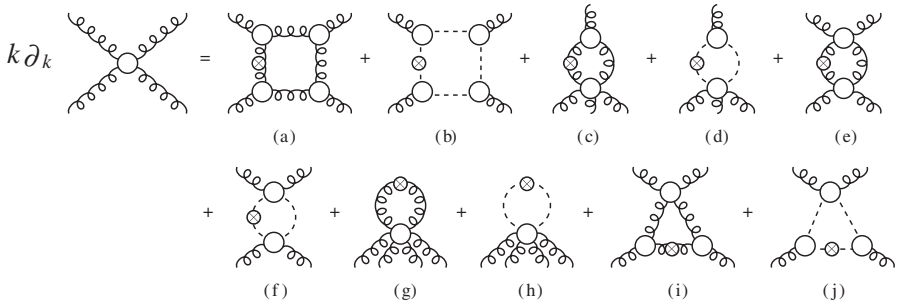

FIG. 8. Functional renormalization group equations for the four-gluon vertex. All internal propagators are taken to be fully dressed. Only one possible insertion of the infrared cutoff function per diagram is shown.

The third term in the second line of (63) puts a bound on $\kappa_{0,4}$,

$$\kappa_{0,4} \leq 2\kappa_{0,2}. \tag{65}$$

Together with the constraint (61), this gives the unique solution

$$\kappa_{0,4} = 2\kappa_{0,2} \tag{66}$$

and

$$\kappa_{0,3} = \tfrac{3}{2}\kappa_{0,2}. \tag{67}$$

Note that the scaling laws (66) and (67) are already generated by the diagrams involving ghosts. Indeed, this is valid for all proper vertices and leads to the unique solution

$$\kappa_{2n,m} = (n-m)\kappa \quad \text{with} \quad \kappa = \kappa_{2,0}, \tag{68}$$

which we now prove: first, we observe that with (68) all diagrams in the FRG have the same leading infrared asymptotics. Let us assume for a moment that (68) is not true for all proper vertices. Then at least one vertex has

$$\kappa_{2n_0,m_0} < (n_0 - m_0)\kappa. \tag{69}$$

The vertex $\Gamma^{(2n_0,m_0)}$ occurs in diagrams of FRG for lower vertex functions $\Gamma^{(2n,m)}$ with $n_0 - n = 1$ or $m_0 - m = 1$. Necessarily, these vertices also satisfy (69) and disagree with (68). Within an iteration, this enforces that *all* vertices with $n \leq n_0$ and $m \leq m_0$ satisfy (69), in particular $\kappa_{0,4}$, $\kappa_{0,3}$, $\kappa_{0,2}$, $\kappa_{2,1}$, $\kappa_{2,0}$. This contradicts the uniqueness of the results (58), (59), (66), and (67) derived above, and hence proves (68).

For the special case of the propagators, this relation has been already derived in [8,10] with the help of additional physical constraints. In [12] the self-consistency of (68) for the whole tower of vertex DSEs has been shown. The dominance of ghost loops in the tower of DSEs is equivalent to the dominance of the Faddeev-Popov determinant over the Yang-Mills action, as proposed in [21]. In the present work we were able to extend these results to a proof of uniqueness based on a self-consistency analysis of the quantum equations of motion.

The above result hinges on a key structure valid for general theories in the presence of a single dynamical scale, and follows already from the structure of the functional DSE (10), Fig. 1, and FRG (13), Fig. 2: any vertex DSE comprises a sum of diagrams proportional to a subset of the bare vertices of the theory at hand. Consistency with the FRG, which only depends on dressed vertices, requires that in all vertex DSEs at least one of these vertices, if dressed, has $\kappa_{\text{vertex}} = 0$. In Landau gauge Yang-Mills theory, this is the ghost-gluon vertex. In general, the above criterion leads to more than one vertex with $\kappa_{\text{vertex}} = 0$.

As an example for this general pattern we extend the pure gauge theory analysis to a YM-Higgs theory. The functional DSE and FRG can be read off from (10) and (13) with $\phi = (A, C, \bar{C}, h)$ and an additional Higgs action $S_{\text{Higgs}} = \frac{1}{2}\int (D_\mu h)^2 + V[h]$. Under the assumption of a single, dynamical mass scale, we deduce a unique relation for a general vertex function $\Gamma^{(2n,m,2l)}$ with n ghost legs, n antighost legs, m gluon legs, h Higgs lines,

$$\kappa_{2n,m,h} = (n-m)\kappa \quad \text{with} \quad \kappa = \kappa_{2,0,0}. \tag{70}$$

In particular, it follows that the Higgs propagator has a constant dressing: $\kappa_h = \kappa_{0,0,2} = 0$, as well as the ϕ^4 coupling $\kappa_{0,0,4} = 0$ required by the presence of vertices with constant dressings in all DSEs. Note that $\kappa_{2n,m,l} = 0$ includes logarithmic scaling. Equation (70) is only valid in the symmetric phase. In the spontaneously broken phase, we expect a massive gauge field propagator, $\kappa_{0,2,0} = -1$, and massive Higgs propagators, $\kappa_h = -1$. Furthermore, as a positive $\kappa \geq 0$ for the ghost signals an unbroken (color) symmetry, we conclude $\kappa \leq 0$ in agreement with the converse of the Higgs theorem [14]. Because of the additional mass scale, some if not all other vertices may scale canonically, i.e. $\kappa_{2n,m,h} = 0$. The present infrared analysis then shows consistently $\kappa_{2n,m,h} \geq 0$; no singular scaling occurs. This is in marked contrast to massless Yang-Mills theory.

In the case of full QCD, including dynamical quarks, the present infrared analysis has interesting consequences which shall be published elsewhere. Finally, we discuss the caveat mentioned at the end of Sec. II. From the above

analysis it is clear that nontrivial cancellations always have to occur in an infinite subset of diagrams. It is hard to see which symmetry should be responsible for such a behavior, as constraints from gauge symmetry, i.e. STIs, are respected by the solution (68).

VI. CONCLUSIONS

In this work we used Dyson-Schwinger equations and functional renormalization group equations to analyze the infrared behavior of proper vertices of $SU(N_c)$ Yang-Mills theory. We have shown that the structure of these functional relations is sufficiently different to generate tight constraints for infrared anomalous dimensions of these vertices. The caveats of this construction have been discussed at the end of Secs. II and V. The constraints are powerful enough to enforce a unique solution (4) and (68) for the infrared behavior of proper vertices in the presence of only one external scale. Thus the Kugo-Ojima criterion (1) is satisfied ensuring a well-defined global color charge. A further consequence is the fixed point behavior of the running coupling in the infrared, since this behavior is implied by the solution (4) via the nonperturbative definitions in Eqs. (35). In turn, the proposal (5) and (6) in [37] is excluded.

We emphasize that both the similarities as well as the differences of DSEs and FRGs were crucial for our results. This structure is certainly useful beyond the present investigation, for example, if devising truncation schemes. Implicitly this criterion was already used in previous works: the coinciding results for the infrared asymptotics from DSE [8–10,12] and FRG [11,22,24] are nontrivial as the functional equations are sufficiently different. This agreement strongly supports the quantitative reliability of the results.

The present consistency analysis not only uniquely fixes the infrared asymptotics but also excludes certain truncation schemes of DSEs and FRGs: e.g. we have shown that truncation schemes of the gluon DSE in Landau gauge Yang-Mills theory relying on an infrared leading behavior of the gluonic one-loop diagram, as e.g. assumed in [44,45], miss the leading infrared behavior. In addition, truncation schemes that assume all terms in the gluon DSE to be equally leading [43] are excluded as well.

It would be desirable to reproduce (4) from lattice QCD. To this end one has to address some caveats in comparing infrared results from the lattice with those of a continuum approach. Lattice simulations are necessarily performed at finite volume and finite lattice spacing, and one has to carefully perform both an infinite volume and a continuum limit extrapolation. These procedures are currently under debate [36,38,47–49]. It is interesting, however, that the procedure of [36] gives $\kappa_{0,2} \approx -1.04$ in agreement with (1). Unfortunately, direct lattice calculations in the infrared scaling region $p < 100$ MeV are extremely expensive in terms of CPU time and have not yet been performed in four dimensional Yang-Mills theory. This is different in three dimensions, where lattice results are in good agreement with the corresponding power-law analysis in the continuum [50].

Furthermore, gauge fixing is implemented differently: in the continuum theory one uses either the Faddeev-Popov method [51] or stochastic gauge fixing [21], whereas on the lattice a gauge fixing functional is extremized. Because of the presence of Gribov copies, this might affect the infrared behavior of Green functions. These effects are currently under investigation in the continuum [21] and on the lattice [30,32,34,52–54]. The effects seem to be much stronger for the ghost than for the gluon propagator. This nicely corresponds to the fact that lattice and continuum solutions agree much better for the gluon than for the ghost.

The present analysis can be extended to full QCD, and reveals an interesting structure. Related results will be published elsewhere.

ACKNOWLEDGMENTS

C. F. is grateful to J. Papavassiliou and J. Rodriguez-Quintero for interesting discussions. We thank R. Alkofer, H. Gies, D. F. Litim, and L. von Smekal for a critical reading of the manuscript and for useful discussions. This work has been supported by the Deutsche Forschungsgemeinschaft (DFG) under Contract No. Fi 970/7-1 and No. GI328/1-2.

[1] C. D. Roberts and A. G. Williams, Prog. Part. Nucl. Phys. **33**, 477 (1994).
[2] R. Alkofer and L. von Smekal, Phys. Rep. **353**, 281 (2001).
[3] C. S. Fischer J. Phys. G **32**, R253 (2006).
[4] D. F. Litim and J. M. Pawlowski, hep-th/9901063.
[5] J. Berges, N. Tetradis, and C. Wetterich, Phys. Rep. **363**, 223 (2002).
[6] J. Polonyi, Central Eur. J. Phys. **1**, 1 (2003).
[7] J. M. Pawlowski, hep-th/0512261.
[8] L. von Smekal, R. Alkofer, and A. Hauck, Phys. Rev. Lett. **79**, 3591 (1997).
[9] D. Zwanziger, Phys. Rev. D **65**, 094039 (2002).
[10] C. Lerche and L. von Smekal, Phys. Rev. D **65**, 125006 (2002).
[11] J. M. Pawlowski, D. F. Litim, S. Nedelko, and L. von Smekal, Phys. Rev. Lett. **93**, 152002 (2004).
[12] R. Alkofer, C. S. Fischer, and F. J. Llanes-Estrada, Phys.

Lett. B **611**, 279 (2005).
[13] T. Kugo, hep-th/9511033.
[14] T. Kugo and I. Ojima, Prog. Theor. Phys. Suppl. **66**, 1 (1979).
[15] D. Zwanziger, Nucl. Phys. **B399**, 477 (1993).
[16] D. Zwanziger, Nucl. Phys. **B364**, 127 (1991).
[17] K. Osterwalder and R. Schrader, Commun. Math. Phys. **31**, 83 (1973).
[18] C. S. Fischer and R. Alkofer, Phys. Lett. B **536**, 177 (2002).
[19] C. S. Fischer and R. Alkofer, Phys. Rev. D **67**, 094020 (2003).
[20] R. Alkofer, W. Detmold, C. S. Fischer, and P. Maris, Phys. Rev. D **70**, 014014 (2004).
[21] D. Zwanziger, Phys. Rev. D **69**, 016002 (2004).
[22] C. S. Fischer and H. Gies, J. High Energy Phys. 10 (2004) 048.
[23] D. F. Litim, J. M. Pawlowski, S. Nedelko, and L. V. Smekal, hep-th/0410241.
[24] J. M. Pawlowski, D. F. Litim, S. Nedelko, and L. von Smekal, AIP Conf. Proc. **756**, 278 (2005).
[25] U. Ellwanger, M. Hirsch, and A. Weber, Z. Phys. C **69**, 687 (1996).
[26] U. Ellwanger, M. Hirsch, and A. Weber, Eur. Phys. J. C **1**, 563 (1998).
[27] B. Bergerhoff and C. Wetterich, Phys. Rev. D **57**, 1591 (1998).
[28] J. Kato, hep-th/0401068.
[29] J. C. Taylor, Nucl. Phys. **B33**, 436 (1971).
[30] A. Cucchieri, Nucl. Phys. **B508**, 353 (1997).
[31] D. B. Leinweber, J. I. Skullerud, A. G. Williams, and C. Parrinello (UKQCD Collaboration), Phys. Rev. D **60**, 094507 (1999); **61**, 079901(E) (2000).
[32] C. Alexandrou, P. de Forcrand, and E. Follana, Phys. Rev. D **63**, 094504 (2001).
[33] K. Langfeld, H. Reinhardt, and J. Gattnar, Nucl. Phys. **B621**, 131 (2002).
[34] S. Furui and H. Nakajima, Phys. Rev. D **70**, 094504 (2004).
[35] A. Sternbeck, E. M. Ilgenfritz, M. Mueller-Preussker, and A. Schiller, Phys. Rev. D **72**, 014507 (2005).
[36] P. J. Silva and O. Oliveira, Phys. Rev. D **74**, 034513 (2006).
[37] P. Boucaud *et al.*, hep-ph/0507104.
[38] F. D. R. Bonnet, P. O. Bowman, D. B. Leinweber, A. G. Williams, and J. M. Zanotti, Phys. Rev. D **64**, 034501 (2001).
[39] J. Gattnar, K. Langfeld, and H. Reinhardt, Phys. Rev. Lett. **93**, 061601 (2004).
[40] D. F. Litim (unpublished).
[41] W. Schleifenbaum, M. Leder, and H. Reinhardt, Phys. Rev. D **73**, 125019 (2006).
[42] P. Watson and R. Alkofer, Phys. Rev. Lett. **86**, 5239 (2001).
[43] J. C. R. Bloch, Few-Body Syst. **33**, 111 (2003).
[44] A. C. Aguilar and A. A. Natale, Int. J. Mod. Phys. A **20**, 7613 (2005).
[45] A. C. Aguilar and A. A. Natale, J. High Energy Phys. 08 (2004) 057.
[46] P. Boucaud *et al.*, J. High Energy Phys. 04 (2003) 005.
[47] A. Cucchieri and T. Mendes, Phys. Rev. D **73**, 071502 (2006).
[48] P. Boucaud *et al.*, hep-lat/0602006.
[49] T. Tok, K. Langfeld, H. Reinhardt, and L. von Smekal, Proc. Sci., LAT2005 (2006) 334.
[50] A. Cucchieri, T. Mendes, and A. R. Taurines, Phys. Rev. D **67**, 091502 (2003).
[51] L. D. Faddeev and V. N. Popov, Phys. Lett. **25B**, 29 (1967).
[52] P. J. Silva and O. Oliveira, Nucl. Phys. **B690**, 177 (2004).
[53] I. L. Bogolubsky, G. Burgio, M. Muller-Preussker, and V. K. Mitrjushkin, Phys. Rev. D **74**, 034503 (2006).
[54] A. Y. Lokhov, O. Pene, and C. Roiesnel, hep-lat/0511049.